

Probing Ligand-binding Pockets of the Mevalonate Pathway Enzymes from *Streptococcus pneumoniae*^{*†}

Received for publication, December 23, 2009, and in revised form, April 2, 2010. Published, JBC Papers in Press, April 19, 2010, DOI 10.1074/jbc.M109.098350

Scott T. Lefurgy^{‡1}, Sofia B. Rodriguez^{‡1}, Chan Sun Park[§], Sean Cahill[¶], Richard B. Silverman[§], and Thomas S. Leyh^{‡2}

From the Departments of [‡]Microbiology & Immunology and [¶]Biochemistry, Albert Einstein College of Medicine, Bronx, New York 10461 and the [§]Department of Chemistry, Department of Biochemistry, Molecular Biology, and Cell Biology, Center for Molecular Innovation and Drug Discovery, and Chemistry of Life Processes Institute, Northwestern University, Evanston, Illinois 60208-3113

Diphosphomevalonate (Mev-pp) is the founding member of a new class of potential antibiotics targeting the *Streptococcus pneumoniae* mevalonate (Mev) pathway. We have synthesized a series of Mev-pp analogues designed to simultaneously block two steps in this pathway, through allosteric inhibition of mevalonate kinase (MK) and, for five of the analogues, by mechanism-based inactivation of diphosphomevalonate decarboxylase (DPM-DC). The analogue series expands the C₃-methyl group of Mev-pp with hydrocarbons of varying size, shape, and chemical and physical properties. Previously, we established the feasibility of a prodrug strategy in which unphosphorylated Mev analogues could be enzymatically converted to the active Mev-pp forms by the endogenous MK and phosphomevalonate kinase. We now report the kinetic parameters for the turnover of non-, mono-, and diphosphorylated analogues as substrates and inhibitors of the three mevalonate pathway enzymes. The inhibition of MK by Mev-pp analogues revealed that the allosteric site is selective for compact, electron-rich C₃-substituents. The lack of reactivity of analogues with DPM-DC provided evidence, counter to the existing model, for a decarboxylation transition state that is concerted rather than dissociative. The Mev pathway is composed of three structurally and functionally conserved enzymes that catalyze consecutive steps in a metabolic pathway. The current work reveals that these enzymes exhibit significant differences in specificity toward R-group substitution at C₃ and that these patterns are explained well by changes in the volume of the C₃ R-group-binding pockets of the enzymes.

Streptococcus pneumoniae, the primary cause of bacterial meningitis and pneumonia, kills over 4000 people daily worldwide and disproportionately affects children and the elderly (1, 2). Antibiotic resistance is a major problem in fighting this organism, with multiple-drug resistance rates as high as 95% in some regions (3). Although vaccines targeting the 7 or 23 most prevalent strains have shown success in reducing disease incidence in developed countries (4), there is a continual need for

new antibiotic strategies to combat unvaccinated strains, which are rapidly filling the biological niches left by the vaccine (5).

The mevalonate (Mev)³ pathway is essential for the survival of *S. pneumoniae* in lung and serum (6). The bacterium uses this pathway to convert Mev to isopentenyl diphosphate, the “building block” of the isoprenoids: a class of 25,000 unique molecules having a wide range of biological functions. The pathway consists of three GHMP family kinases: Mev kinase (MK), phosphomevalonate kinase (PMK) and diphosphomevalonate decarboxylase (DPM-DC) (Fig. 1) (7). Mutations that knock out genes in this pathway kill the organism *in vivo*, suggesting that *S. pneumoniae* cannot obtain the necessary precursors or downstream products from the host (6). In principle, each of the three enzymes is an antibiotic target, because inhibition of any of them prevents the production of isopentenyl diphosphate. We have shown that *S. pneumoniae* MK is potently ($K_i = 500$ nM) allosterically inhibited by diphosphomevalonate (Mev-pp), the third compound in the pathway, whereas the human MK homologue is not (8). Thus, the allosteric site provides an opportunity to selectively target the bacterium. The *S. pneumoniae* MK crystal structure revealed a pore at the subunit interface with excellent charge- and shape-complementarity to Mev-pp that may be the allosteric site.

In an effort to enhance the inhibitory properties of Mev-pp for use as an antibiotic, we have built a series of ten Mev analogues (9) in which the C₃-methyl group has been altered to other hydrocarbon substituents (Table 1). Five of the analogues have linear and branched alkyl groups at C₃ that act as structural probes for the MK allosteric site and the active sites of the three GHMP kinases. The remaining five analogues resemble the alkyl series but also have the potential to act as mechanism-based inhibitors of DPM-DC.

In the DPM-DC mechanism, the C₃-hydroxyl of Mev-pp is phosphorylated by ATP, generating p-Mev-pp, which ionizes, leaving a carbocation on C₃; decarboxylation is thought to follow rapidly (10). Abeles and coworkers have provided evidence

* This work was supported, in whole or in part, by National Institutes of Health Grant AI 068989.

† The on-line version of this article (available at <http://www.jbc.org>) contains supplemental text, Fig. S1, Table S1, and Schemes S1–S3.

¹ Both authors contributed equally to this work.

² To whom correspondence should be addressed: 1300 Morris Park Ave., Bronx, NY 10461. Tel.: 718-430-2858; Fax: 718-430-8711; E-mail: thomas.leyh@einstein.yu.edu.

³ The abbreviations used are: Mev, mevalonate; Mev-p, phosphomevalonate; Mev-pp, diphosphomevalonate; p-Mev-pp, 3-phospho-5-diphosphomevalonate; DPM-DC, diphosphomevalonate decarboxylase; HMBC, heteronuclear multiple-bond connectivity; HSQC, heteronuclear single quantum coherence; LDH, lactate dehydrogenase; 2-ME, β -mercaptoethanol; MK, Mev kinase; PEP, phosphoenolpyruvate; PK, pyruvate kinase; PMK, phosphomevalonate kinase; unit, 1 μ mol of product formed per minute at a saturating concentration of one or more substrates; X, the Mev analogue series; X-p, the phosphomevalonate analogue series; X-pp, the diphosphomevalonate analogue series.

S. pneumoniae Mevalonate Pathway Enzymes

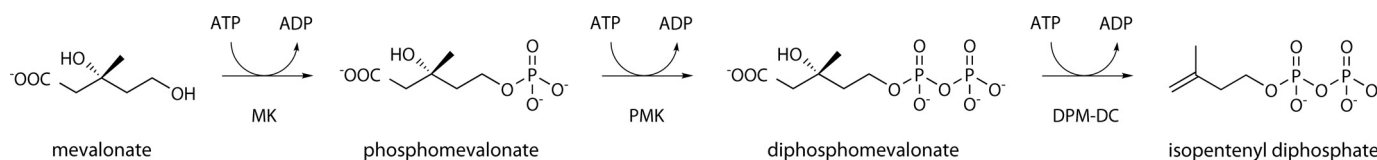


FIGURE 1. **The mevalonate pathway.** The conversion of mevalonate to isopentenyl diphosphate occurs in three ATP-dependent steps catalyzed by GHMP family kinases: MK, mevalonate kinase; PMK, phosphomevalonate kinase; DPM-DC, diphosphomevalonate decarboxylase.

with the mammalian enzyme that a carbocation must form during turnover by showing that substitution of the C₃-methyl group with a hydrogen or a fluoromethyl group causes the reaction to halt after phosphorylation, implying that the electron-donating methyl group is required to stabilize the carbocation inductively (10). To exploit the potential carbocation formation for DPM-DC inhibition, we replaced the C₃-methyl group with substituents that could undergo resonance with the carbocation, thereby setting up an electrophilic site for nucleophilic attack by the enzyme (Fig. 2). Because the inhibitors are structurally related to Mev·pp, we expected that they might also inhibit MK through binding at the allosteric site. By targeting two steps in the same pathway, such molecules are expected to have enhanced antibiotic potency.

We now report the chemical and chemoenzymatic synthesis of the Mev·pp analogue series, the kinetic parameters of the Mev, Mev·p, and Mev·pp analogues as substrates of their three respective Mev pathway GHMP kinases, and the inhibition of MK and DPM-DC by Mev·pp analogues, noting their potential as antibiotics and the substrate-binding features of the enzyme family that they reveal.

EXPERIMENTAL PROCEDURES

General Materials and Methods—Lactate dehydrogenase (LDH, rabbit muscle), pyruvate kinase (PK, rabbit muscle), and alkaline phosphatase (calf intestine) were purchased from Roche Applied Science and treated as described previously (11). ATP, ADP, NADH, phosphoenolpyruvate (PEP), β-mercaptoethanol (2-ME), (*R,S*)-mevalonate (Mev), and triethylamine were purchased from Sigma. NaCl, KCl, Hepes, Tris, MgCl₂, KOH, glycerol, and Luria-Bertani Miller media were purchased from Fisher Scientific. Isopropyl-1-thio-β-D-galactopyranoside was purchased from Labscientific, Inc. Q-Sepharose Fast Flow ion-exchange, Chelating Sepharose Fast Flow, and Glutathione-Sepharose 4 Fast Flow resins were purchased from Amersham Biosciences. Anion-exchange resin AG MP-1 was purchased from Bio-Rad. YM-10 membranes were purchased from Millipore. Competent *Escherichia coli* BL21(DE3) was purchased from Novagen. Racemic mevalonolactone analogues ((*R,S*)-X), *Streptococcus pneumoniae* MK, PMK, DPM-DC, and *Staphylococcus aureus* MK were prepared as described previously (9, 11). Chromatography was carried out using an ÄKTA fast-protein liquid chromatography system (Amersham Biosciences). Spectrophotometric measurements were carried out using a Cary 100 or 400 UV-visible spectrophotometer (Varian, Inc.). Fluorometric measurements were carried out using a Cary Eclipse fluorometer (Varian, Inc.).

Chemical Nomenclature—In the description of kinetic experiments, the substrate analogues (in free acid form) are referred to by boldface numbers that correspond to the struc-

tures given in Table 1. Where appropriate, numbers are appended with “·p” or “·pp” to indicate the number of phosphates on the C₅-hydroxyl. For example, **6·pp** refers to the 5'-diphosphorylated form of the vinyl analogue (see Table 1). A group of analogues of a particular phosphorylation state is referred to using a boldface X in place of the number (*i.e.* X, X·p, or X·pp).

Enzymatic Synthesis of Stereochemically Pure Substrates of the Mevalonate Pathway—A series of (*R,S*)-mevalonolactone analogues ((*R,S*)-X) were synthesized as racemic mixtures as described (9). Approximately 25 mg of each lactone was treated with five equivalents of KOH at 37 °C for 1 h to convert it to the corresponding carboxylate. The solution was then adjusted to pH 7.0 with 1 M HCl and diluted with Hepes/K⁺ (50 mM, pH 7.0) and MgCl₂ (1.0 mM) to a final concentration of ~240 mM in 750 μl. Concentration of the *R*-isomer was determined by enzymatic assay (see below).

Stereochemically pure mono- and diphosphorylated Mev analogues ((*R*)-X·p and (*R*)-X·pp (X = **1**, **3**, **6**, and **7**)) were enzymatically synthesized from racemic Mev analogues (*R,S*)-X in successive steps catalyzed by MK and PMK. The first phosphorylation reaction contained *S. pneumoniae* MK (0.350 μM), (*R,S*)-X (~7.5 mM), ATP (4.5 mM), PK (10 units/ml), PEP (10 mM), 2-ME (20 mM), MgCl₂ (5.5 mM), and Hepes/K⁺ (50 mM, pH 8.0) After 72 h at room temperature, 98% of the starting material had been converted to the (*R*)-X·p analogue. The second phosphorylation was initiated by the addition of PMK (0.28 μM) and PEP (1.0 mM) to the reaction mixture, and this reaction achieved 99% conversion to (*R*)-X·pp analogue after ~24 h. Because (*R,S*)-**9** was known to be a slow substrate for *S. pneumoniae* MK, the production of (*R*)-**9**·pp was facilitated using a one-pot reaction that included *S. aureus* MK, which is weakly inhibited by Mev·pp, and PMK. The reaction was completed in 36 h. (*R*)-**9**·p was synthesized as described above, but starting from (*R*)-**9**. (*R*)-X compounds (X = **1**, **3**, **6**, **7**, and **9**) were generated by removing the pyrophosphoryl moiety from two-thirds of the purified (see below) (*R*)-X·pp using alkaline phosphatase. The reaction mixtures contained: alkaline phosphatase (2.5 units/ml), (*R*)-X·pp (2.4 mM), Tris/HCl (50 mM, pH 8.5) at 37 °C (98% conversion to product was reached in 1 h). The (*R*)-X analogues were found to lactonize upon purification (see below) and were saponified to the carboxylates as described above.

Reaction progress and analogue concentration were monitored by enzymatic assay (12). MK, PMK, and DPM-DC produce ADP in the presence of their respective substrates; ADP formation was measured spectrophotometrically at 339 nm by stoichiometrically coupling (1:1) ADP production to NADH oxidation using the well established PK/LDH-coupled assay

S. pneumoniae Mevalonate Pathway Enzymes

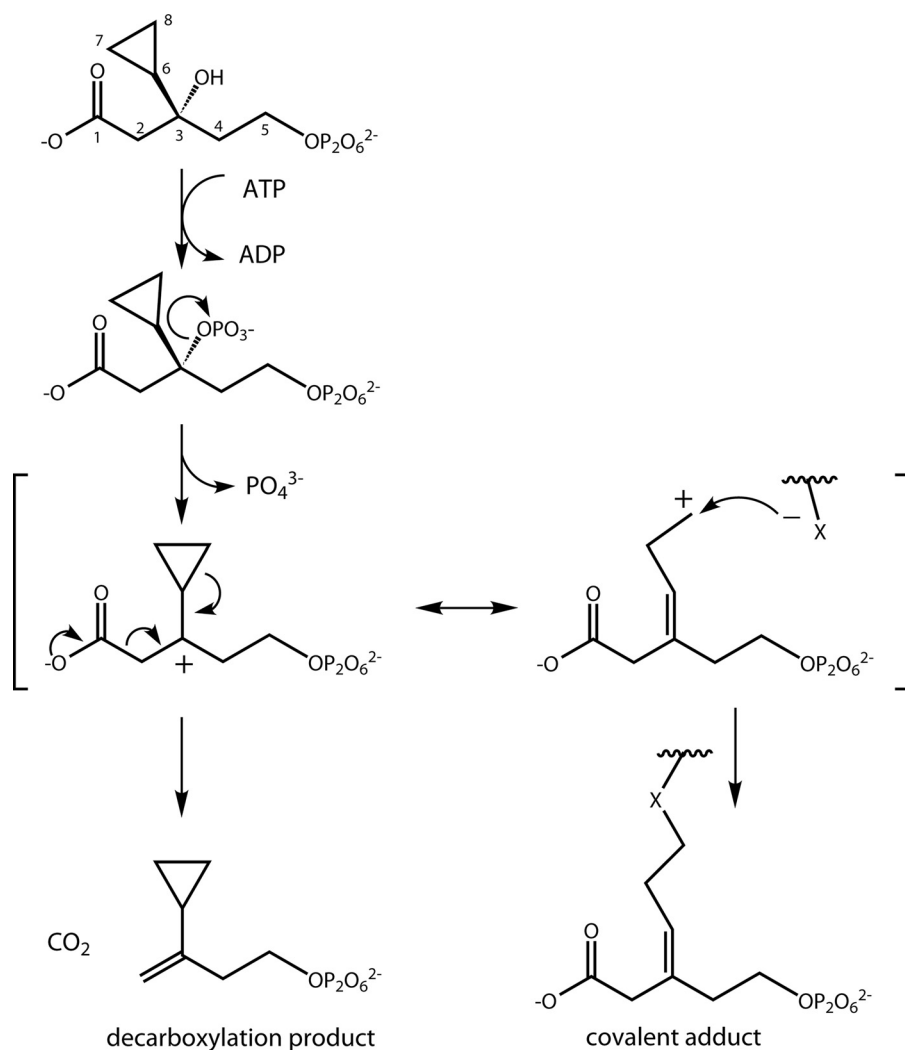


FIGURE 2. **DPM-DC inactivation hypothesis.** The dissociative model of Mev-pp decarboxylation (shown for the **9-pp** analogue) begins with phosphorylation of the C₃-OH by ATP. Phosphate then ionizes, leaving a C₃ carbocation, which either rapidly decarboxylates to form the double-bonded product (left resonance form) or, in the case of analogues **6-pp** through **10-pp**, rearranges and is quenched by a nucleophile on the protein surface (right resonance form), forming a covalent adduct. Opening the cyclopropyl ring of the **9-pp** analogue results in a homoallyl carbocation that is stabilized, relative to the ring-intact carbocation, as a result of the release of the ~27 kcal/mol ring strain (29, 30).

system (13). The assay conditions were as follows: *S. pneumoniae* MK, PMK, or DPM-DC (1.0 μM), reaction mixture or analogue (5 μl), ATP (3.0 mM), MgCl₂ (4.0 mM), HEPES/K⁺ (50 mM, pH 8.0), KCl (50 mM), PK (6.0 units/ml), LDH (12 units/ml), PEP (5.0 mM), 2-ME (10 mM), and NADH (200 μM, Δε = 6.22 mM⁻¹cm⁻¹). For each mole of (R,S)-X in the initial reaction, 0.5 mol of product was produced, representing a biologically relevant (R)-isomer. ADP (2.0 mM) was added at the end of synthesis reactions to completely convert PEP to pyruvate, facilitating purification of the phosphorylated Mev species.

Purification of R-Mevalonate, 5-Monophosphate, and 5-Diphosphate Analogues—A reaction mixture containing (R)-X, (R)-X·p, or (R)-X·pp was separated from enzymes by passing the solution through a YM-10 membrane. The filtrate was loaded onto an anion-exchange resin (AG MP-1, 35 ml) equilibrated with HEPES/K⁺ (10 mM, pH 7.5), washed five times with equilibration buffer, and eluted using a linear KCl gradient (0–1.0 M, 750 ml, 2 ml/min). (R)-X, (R)-X·p, and (R)-X·pp ana-

logues eluted at 0.2, 0.285, and 0.33 M KCl, respectively, and contained <1% nucleotide. Each purified analogue was desalted by loading onto an anion-exchange resin (Q-Sepharose Fast Flow, 5 ml) and washing (10 mM) and eluting (1.2 M) with triethylamine/HCO₃⁻ (pH 7.0). Excess triethylamine was removed by rotary evaporation, washing with 100% methanol (25 ml, six times) and ultrapure water (25 ml, three times). Solution pH was adjusted to 7.0 with HCl, and the concentration of the analogue was determined by enzymatic assay.

Determination of Initial Rate Constants—Initial rate constants of MK, PMK, and DPM-DC reactions with substrate analogues were determined by a progress curve method. Complete MK reaction progress curves were obtained by monitoring absorbance at 398 nm. Products were removed by including PMK and DPM-DC in the reaction mixture to prevent possible product inhibition; therefore, three molar equivalents of NADH are oxidized per MK substrate. (R)-1, -3, -6, -7, and -9 were previously shown to be substrates for MK (9). The concentration of acceptor (Mev or analogue) and MK varied according to the kinetic constants of the acceptor. The conditions were as follows: Mev (135 μM), MK (100 nM); **1** (400 μM), MK (500 nM); **3** (1.0 mM), MK (10 μM); **6** (400 μM), MK (500 nM); **7** (400 μM), MK (1.0 μM); and **9** (600 μM), MK (1.0 μM). The reaction mixture contained:

ATP (5.0 mM, 30·K_m), MgCl₂ (6.0 mM), HEPES/K⁺ (50 mM, pH 8.0), KCl (50 mM), PK (5.0 units/ml), LDH (10 units/ml), PEP (4.0 mM), 2-ME (10 mM), and NADH (7.0 mM, Δε₃₉₈ = 0.136 mM⁻¹cm⁻¹); T = 25 ± 2 °C. The concentrations of the coupling enzymes PMK and DPM-DC were selected to minimize their contribution to the lag time of the assay (14); consequently they varied according to the kinetic constants of these enzymes toward a given acceptor. The concentrations, given in the format (acceptor, [PMK] (μM), [DPM-DC] (μM)), were as follows: (Mev, 0.15, 0.30), (**1**, 3.0, 2.0), (**3**, 15, 15), (**6**, 1.5, 1.0), (**7**, 2.0, 3.0), and (**9**, 3.0, 2.0). The maximum concentrations of (R)-1, -3, -6, -7, and -9 that could reasonably be achieved in the assay were too low relative to their K_m to obtain precise K_m values; consequently, only V/K values were determined (see Table 1).

(R,S)-2, -4, -5, -8, and -10 proved to be extremely poor substrates for MK; product was not detected under the following conditions: (R,S)-X (1.0 mM), MK (10 μM), PMK (1.0 μM),

DPM-DC (2.0 μM), ATP (8.0 mM, $9.5 \cdot K_m$), MgCl_2 (9.0 mM), Hepes/ K^+ (50 mM, pH 8.0), KCl (50 mM), PK (6.0 units/ml), LDH (12 units/ml), PEP (4.0 mM), 2-ME (10 mM), and NADH (2.0 mM, $\Delta\epsilon_{386} = 0.61 \text{ mM}^{-1}\text{cm}^{-1}$); $T = 25 \pm 2^\circ\text{C}$. No diphosphorylated product was detected over a 4-h period. The limit of detection of the instrument ($\Delta A_{386} = 0.025 \text{ h}^{-1}$) corresponds to a maximum rate of $0.067 \mu\text{M min}^{-1}$.

PMK reaction progress curves were measured by monitoring absorbance at 339 nm. The product was removed by including DPM-DC in the reaction mixture to prevent possible product inhibition; therefore, two molar equivalents of NADH are produced per PMK substrate. The concentration of analogue and PMK varied in each experiment: Mev

•p

 (100 μM), PMK (10 nM); **1•p** (600 μM), PMK (150 nM); **3•p** (600 μM), PMK (2.0 μM); **6•p** (600 μM), PMK (75 nM); **7•p** (600 μM), PMK (100 nM); and **9•p** (600 μM), PMK (500 nM). The reaction mixture contained: ATP (4.0 mM, $30 \cdot K_m$), MgCl_2 (5.0 mM), Hepes/ K^+ (50 mM, pH 8.0), KCl (50 mM), PK (6.0 units/ml), LDH (12 units/ml), PEP (4.0 mM), 2-ME (10 mM), and NADH (2.0 mM, $\Delta\epsilon_{386} = 0.61 \text{ mM}^{-1}\text{cm}^{-1}$); $T = 25 \pm 2^\circ\text{C}$. The concentration of DPM-DC varied according to the kinetic constants for a given analogue. The concentrations, given as (**acceptor**, [DPM-DC] (μM)), were as follows: (**Mev•p**, 0.50), (**1**, 3.0), (**3**, 20); (**6**, 1.5), (**7**, 1.5), (**9**, 3.0). Analogues **2•p**, **4•p**, **5•p**, **8•p**, and **10•p** could not be produced enzymatically using MK and were not tested.

Complete DPM-DC reaction progress curves for (*R*)-**1•pp**, **3•pp**, **6•pp**, **7•pp**, and **9•pp** were measured by the change in fluorescence upon oxidation of NADH ($\lambda_{\text{Ex}} = 339 \text{ nm}$ and $\lambda_{\text{Em}} = 466 \text{ nm}$). The amount of NADH oxidized during the incubation was calculated by comparison to a standard curve; NADH fluorescence gave a linear response up to 10 μM . The concentration of analogue and DPM-DC varied in each experiment: Mev•pp (5.0 μM), DPM-DC (2.5 nM); **1•pp** (3.0 μM), DPM-DC (5.0 nM); **3•pp** (6.0 μM), DPM-DC (30 nM); **6•pp** (6.0 μM), DPM-DC (2.5 nM); **7•pp** (6.0 μM), DPM-DC (15 nM); and **9•pp** (2.6 μM), DPM-DC (30 nM). The reaction mixture contained: ATP (4.0 mM, $55 \cdot K_m$), MgCl_2 (5.0 mM), Hepes/ K^+ (50 mM, pH 8.0), KCl (50 mM), PK (4.0 units/ml), LDH (8.0 units/ml), PEP (2.0 mM), 2-ME (10 mM), and NADH (13 μM); $T = 25 \pm 2^\circ\text{C}$. (*R,S*)-**2•pp**, **4•pp**, **5•pp**, **8•pp**, and **10•pp** progress curves were acquired by monitoring absorbance at 339 nm to accommodate the higher substrate concentrations needed to determine K_m . The concentration of the (*R,S*) analogue ((*R*)-isomer) and DPM-DC varied in each experiment: **2•pp** (17 μM), DPM-DC (3.0 μM); **4•pp** (64 μM), DPM-DC (3.2 μM); **5•pp** (17 μM), DPM-DC (800 nM); **8•pp** (13 μM), DPM-DC (100 nM); and **10•pp** (11 μM), DPM-DC (6.0 μM). The reaction mixture contained: ATP (2.0 mM, $30 \cdot K_m$), MgCl_2 (3.0 mM), Hepes/ K^+ (50 mM, pH 8.0), KCl (50 mM), PK (2.0 units/ml), LDH (4.0 units/ml), PEP (2.0 mM), 2-ME (10 mM), and NADH (0.2 mM, $\Delta\epsilon_{339} = 6.22 \text{ mM}^{-1}\text{cm}^{-1}$); $T = 25 \pm 2^\circ\text{C}$. At the end of each reaction, additional equivalents of the analogue and NADH were added to the cuvette, and a second progress curve was obtained; upon comparison to the first curve, it was found to be identical, indicating the absence of product inhibition at the concentrations of product generated by the reaction.

Progress Curve Analysis—Values of k_{cat} and K_m for each enzyme with its substrates were determined by statistically fit-

ting complete reaction progress curves to the integrated Michaelis-Menten equation (Equation 1), using a FORTRAN77 program of Cleland (15) adapted by one of us (S. T. L.) for this purpose (available upon request). Prior to analysis, the linear background ATP hydrolysis was subtracted from the curve, and the data were manually truncated to remove the lag in NADH oxidation due to coupling enzymes. Absorbance values were normalized to the minimum absorbance value and converted to substrate concentrations (S_t) using the extinction coefficient of NADH and equivalents of ADP produced in each reaction (see above). The initial substrate concentration (S_0) was taken from the corrected, normalized absorbance at $t = 0$.

$$t = \frac{1}{k_{\text{cat}}[E]} \left[K_m \ln \frac{S_0}{S_t} + (S_0 - S_t) \right] \quad (\text{Eq. 1})$$

Fitted parameters k_{cat} and K_m (p_n) and associated errors from two or three independent progress curves of each enzyme-substrate pair were averaged (16). Mean parameter values (\hat{p}) and their associated errors ($\sigma_{\hat{p}}$) were determined using Equations 2 and 3. Weighting factors (a_n) were obtained from Equation 4, where the variance (σ_n^2) is the square of the standard deviation (σ_n) of the least-squares fitted parameter.

$$\hat{p} = a_1 p_1 + a_2 p_2 + a_3 p_3 \quad (\text{Eq. 2})$$

$$V(\hat{p}) = a_1^2 \sigma_1^2 + a_2^2 \sigma_2^2 + a_3^2 \sigma_3^2 \quad (\text{Eq. 3})$$

$$a_n = \frac{1/\sigma_n^2}{(1/\sigma_1^2) + (1/\sigma_2^2) + (1/\sigma_3^2)} \quad (\text{Eq. 4})$$

S. pneumoniae DPM-DC Homology Model with Mev•pp—A homology model of the *S. pneumoniae* enzyme was generated in Swiss PDB Viewer (17) from the crystal structure of *S. pyogenes* DPM-DC (70% sequence identity, PDB: 2GS8). The fifteen active-site residues used to position Mev•pp in the model are completely conserved in the two sequences. Mev•pp was manually positioned using the criteria of Byres *et al.* (18), which were used to position Mev•pp in the apo *Trypanosoma brucei* DPM-DC structure (PDB: 2HKE). To facilitate comparison of the two structures, the *T. brucei* structure was aligned with the *S. pneumoniae* homology model, using PyMOL (19). The Mev•pp ligand was then positioned using the criteria below to determine placement of the terminal phosphate, the C_1 -carboxylate, and the C_3 -hydroxyl. The terminal phosphate of Mev•pp in the *T. brucei* model was positioned where a sulfate is bound by four highly conserved residues in the crystal structure; two of the four residues coordinating this sulfate are conserved in *S. pneumoniae* DPM-DC (Lys-22 and Gly-140), the third is conservatively replaced (Lys-74 for Arg-77), and Arg-186 replaces the fourth residue, Thr-200. In the *T. brucei* structure, the helix containing Arg-77 is positioned closer to the sulfate than the corresponding helix in *S. pneumoniae*, such that the corresponding Lys-74 is 9 Å from the sulfate. It is therefore possible that Arg-186 functionally replaces Lys-74. With these considerations, the terminal phosphate of Mev•pp was placed within hydrogen bond distance (2.5–4.0 Å) of Lys-22, Gly-140, and Arg-186 in the *S. pneumoniae* model, guided by the structural alignment. The C_1 -carboxylate, which in the *T.*

S. pneumoniae Mevalonate Pathway Enzymes

brucei model is coordinated by Arg-149, was positioned within 4 Å of the corresponding Arg-144 and the conserved Ser-141 side chain in the *S. pneumoniae* model. This Ser residue is conserved in GHMP kinases that bind Mev, Mev·p, and Mev·pp and forms a hydrogen bond with the C₁-carboxylate in all three ligand-bound crystal structures (PDB: 2HFU, 2O12, and 3GON). The C₃-hydroxyl group, which is the nucleophile that attacks the ATP γ-phosphate, is positioned in the *T. brucei* model near Asp-293, a highly conserved residue in GHMP kinases that assists phosphoryl transfer by deprotonating the C₃-hydroxyl (18). In the *S. pneumoniae* model, the C₃-hydroxyl was positioned within 3.5 Å of Asp-276 and points toward the conserved ATP-binding pocket. To make these contacts, the C₂–C₃ bond angle of Mev·pp was rotated ~120° relative to its conformation in the MK crystal structure. This change puts the C₁-carboxylate antiperiplanar to the C₃-hydroxyl that departs during decarboxylation, making the optimal geometry for a concerted elimination reaction, one of the possible mechanisms for this enzyme. Positioned in this way, the C₃-methyl group of Mev·pp points directly into a large, water-filled cavity composed of Ala-15, Lys-18, Tyr-19, Trp-20, Ser-185, Met-189, Met-236, Tyr-249, and Asp-276. This pocket is highly conserved in each of the seven DPM-DC crystal structures available in the PDB.

Allosteric Inhibition of Mevalonate Kinase by Mev·pp Analogues—The IC₅₀ values for the diphosphorylated analogues were measured by titration. The reaction mixture included: MK (10 nM), Mev (135 μM, 5·K_m), ATP (5.0 mM, 6·K_m), MgCl₂ (6.0 mM), Hepes/K⁺ (50 mM, pH 8.0), KCl (50 mM), PK (6.0 units/ml), LDH (12 units/ml), PEP (5.0 mM), 2-ME (10 mM), and NADH (200 μM, Δε₃₃₉ = 6.22 mM⁻¹cm⁻¹); T = 25 ± 2 °C. If no inhibition was observed at 250 μM, the IC₅₀ of that compound was not determined. Initial velocities (v) were measured during consumption of the first 8–10% of limiting substrate at inhibitor concentrations ([I]) that were increased until 20–50% inhibition was obtained. The analogue IC₅₀ values were determined by fitting the v versus [I] data points to Equation 5, where uninhibited velocity is given by v_o.

$$v = \frac{v_o}{1 + [I]/IC_{50}} \quad (\text{Eq. 5})$$

To determine the inhibition mechanism and kinetic constants for **6·pp** and **9·pp** inhibition, initial rates were measured for a matrix of conditions comprising three inhibitor concentrations and three or four fixed-variable substrate concentrations with the other substrate held constant. When Mev was varied, the assay contained MK (2.5 nM), Mev (0.5 to 3.7·K_m), ATP (3.0 mM, 3.6·K_m), MgCl₂ (4.0 mM), Hepes/K⁺ (50 mM, pH 8.0), KCl (50 mM), PK (3.0 units/ml), LDH (6.0 units/ml), PEP (5.0 mM), 2-ME (10 mM), NADH (10 μM), **6·pp** (0, 15, 40 μM), or **9·pp** (0, 20, 60 μM); T = 25 ± 2 °C. The reactions were initiated with Mev, and after each measurement, during which 5–7% of the substrate was consumed, Mev was successively added to the cuvette. When ATP was varied, the assay contained MK (2.5 nM), Mev (135, 5·K_m), ATP (1 to 5·K_m), MgCl₂ ([nucleotide] plus 1 mM),

Hepes/K⁺ (50 mM, pH 8.0), KCl (50 mM), PK (6.0 units/ml), LDH (12 units/ml), PEP (5.0 mM), 2-ME (10 mM), NADH (10 μM), and **6·pp** or **9·pp** (0, 25, 50 μM); T = 25 ± 2 °C. The reaction was initiated by addition of Mev; initial velocities were measured during consumption of the first 5–7% of the concentration-limiting substrate (Mev). Under these conditions, product inhibition by Mev·p was not observed. The initial velocities, substrate concentrations, and inhibitor concentrations were fit to a noncompetitive inhibition model (Equation 6).



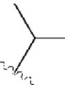
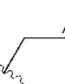
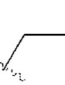
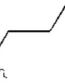




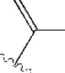
$$V = \frac{V_{\max}[S]}{K_m \left(1 + \frac{[I]}{K_{is}}\right) + [S] \left(1 + \frac{[I]}{K_{ii}}\right)} \quad (\text{Eq. 6})$$

Diphosphomevalonate Decarboxylase Electrophilic Inactivation—Inactivation of *S. pneumoniae* DPM-DC by putative **X·pp** electrophiles (X = **6–10**) was tested as a function of turnover. Reactions were initiated by the addition of the diphosphorylated analogues and allowed to proceed until >1000 enzyme-equivalents of product had formed. Inactivation was measured as a percent reduction in velocity after 1000 turnovers at saturating substrate. The concentrations of **X·pp** and DPM-DC in each assay were: **6·pp** (400 μM, 133·K_m), DPM-DC (10 nM); **7·pp** (350 μM, 200·K_m), DPM-DC (10 nM); **8·pp** (874 μM, 156·K_m), DPM-DC (200 nM); **9·pp** (400 μM, 200·K_m), DPM-DC (100 nM); and **10·pp** (400 μM, 26.6·K_m), DPM-DC (200 nM). The reaction mixture contained: ATP (4.0 mM, 54·K_m), MgCl₂ (5.0 mM), Hepes/K⁺ (50 mM, pH 8.0), KCl (50 mM), PK (3.0 units/ml), LDH (6.0 units/ml), PEP (2.0 mM), 2-ME (10 mM), and NADH (200 μM, Δε = 6.22 mM⁻¹cm⁻¹); T = 25 ± 2 °C. The activity of DPM-DC over the course of 1000 turnovers in the presence of Mev·pp was used as a negative control for inactivation.

Monitoring Fate of the Cyclopropyl Ring during DPM-DC Turnover—¹H NMR was used to monitor the **9·pp** cyclopropyl ring during DPM-DC turnover. The reaction was initiated by the addition of **9·pp** (3.0 mM) and also contained: DPM-DC (10 μM), ATP (3.0 mM, 40·K_m), MgCl₂ (4.0 mM), Hepes/K⁺ (50 mM, pH 8.0), KCl (50 mM), PK (6.0 units/ml), LDH (12 units/ml), PEP (5.0 mM), 2-ME (10 mM), NADH (4.0 mM), D₂O (50 μl), and 3-trimethylsilyl propionate (3.0 μl) as an internal marker. The ¹H NMR spectrum of the reaction mixture was taken at t₀ and every 7 min until >95% conversion of product was reached. ¹H-¹³C HSQC and HMBC spectra were taken on the final product to identify carbon functional groups and assign the chemical shifts of cyclopropyl protons.

All NMR experiments were performed at 25 °C on a Bruker DRX 600-MHz spectrometer equipped with a 5-mm inverse triple resonance probe. One-dimensional proton spectra were collected with 64 scans of 64,000 points over 20 ppm and a total recycle delay of 6 s. The residual water in the spectrum was removed using pre-saturation of the HOD signal. Spectra were processed with an exponential line broadening of 1 Hz, and the proton chemical shifts were referenced to internal 3-trimethylsilyl propionate. Two-dimensional ¹H-¹³C HSQC spectra were typically collected with 1,000 and 256 complex points in t₂ (¹H) and t₁ (¹³C), respectively, with 64 scans per t₁ point and a recycle delay of 1.3 s. The HSQC experiments used a proton sweep width of 12 ppm and a ¹³C sweep width of 200 ppm with the ¹H and ¹³C carriers set to 4.7

TABLE 1
Initial rate parameters of *S. pneumoniae* Mev pathway enzymes with Mev analogues

Name	R group	MK	PMK			DPM-DC		
		$k_{\text{cat}}/K_m \text{X}^{\text{c}}$ ($\mu\text{M}^{-1} \text{sec}^{-1}$)	$K_m \text{X-p}^{\text{c}}$ (μM^{-1})	k_{cat} (sec^{-1})	$k_{\text{cat}}/K_m \text{X-p}$ ($\mu\text{M}^{-1} \text{sec}^{-1}$)	$K_m \text{X-pp}^{\text{c}}$ (μM^{-1})	k_{cat} (sec^{-1})	$k_{\text{cat}}/K_m \text{X-pp}$ ($\mu\text{M}^{-1} \text{sec}^{-1}$)
Mev		$\frac{0.22(1)^{\text{a}}}{1}$	$\frac{7.9(1)}{1}$	$\frac{8.3(1)}{1}$	$\frac{1.0(1)}{1}$	$\frac{1.2(1)}{1}$	$\frac{5.6(1)}{1}$	$\frac{4.5(1)}{1}$
1		$\frac{0.0013(1)}{0.0059}$	$\frac{630(1)}{78}$	$\frac{11(1)}{1.3}$	$\frac{0.017(1)}{0.017}$	$\frac{1.5(1)}{1.3}$	$\frac{1.3(0.1)}{0.23}$	$\frac{0.86(1)}{0.19}$
2		n.d. ^b	● ^c	●	●	$\frac{16(1)}{13}$	$\frac{0.018(3)}{0.0032}$	$\frac{0.0012(1)}{0.00027}$
3		$\frac{0.000041(1)}{0.00019}$	— ^d	—	$\frac{0.0012(1)}{0.0012}$	$\frac{2.8(1)}{2.3}$	$\frac{0.39(1)}{0.069}$	$\frac{0.14(1)}{0.031}$
4		n.d.	●	●	●	$\frac{29(3)}{24}$	$\frac{0.024(3)}{0.0043}$	$\frac{0.00081(1)}{0.00018}$
5		n.d.	●	●	●	—	—	$\frac{0.012(1)}{0.0027}$
6		$\frac{0.0033(1)}{0.015}$	$\frac{210(1)}{27}$	$\frac{5.2(2)}{0.63}$	$\frac{0.025(1)}{0.025}$	$\frac{1.7(1)}{1.4}$	$\frac{3.2(2)}{0.57}$	$\frac{1.9(1)}{0.42}$
7		$\frac{0.0031(1)}{0.014}$	$\frac{500(1)}{63}$	$\frac{4.0(1)}{0.48}$	$\frac{0.0080(1)}{0.0080}$	$\frac{2.9(1)}{2.4}$	$\frac{1.3(1)}{0.23}$	$\frac{0.43(1)}{0.095}$
8		n.d.	●	●	●	$\frac{6.3(1)}{5.3}$	$\frac{0.21(1)}{0.038}$	$\frac{0.034(3)}{0.0076}$
9		$\frac{0.00016(1)}{0.00073}$	—	—	$\frac{0.0027(1)}{0.0027}$	$\frac{1.0(1)}{0.83}$	$\frac{0.27(1)}{0.048}$	$\frac{0.26(1)}{0.058}$
10		n.d.	●	●	●	—	—	$\frac{0.00054(1)}{0.00012}$

^a Parentheses indicate \pm S.D. as a percentage of the parameter value. Denominator indicates parameter value relative to native acceptor substrate.

^b Product not detected (see "Experimental Procedures").

^c Substrate was not tested.

^d Poor substrate; initial rate parameters could not determined (see "Experimental Procedures").

^e X, X-p, and X-pp refer to the non-, mono-, and diphosphorylated mevalonate analogues, respectively.

and 75 ppm, respectively. Two-dimensional ^1H - ^{13}C HMBC spectra were typically collected with 1,000 and 256 complex points in t_2 (^1H) and t_1 (^{13}C), respectively, with 192 scans per t_1 point and a recycle delay of 1.3 s. The HMBC experiments used a proton sweep width of 12 ppm and a ^{13}C sweep width of 225 ppm with the ^1H and ^{13}C carriers set to 4.7 and 100 ppm, respectively.

RESULTS AND DISCUSSION

Synthesis of Mev, Mev-p, and Mev-pp Analogues—The initial steps of isoprenoid biosynthesis are catalyzed by three GHMP

family kinases (MK, PMK, and DPM-DC), which convert Mev to isopentenyl diphosphate, through the metabolic intermediates Mev-p and Mev-pp. Because our goal was to use Mev analogues as prodrugs to generate Mev-pp analogues in the cell, knowledge of the substrate selectivities of these enzymes is helpful in designing potential inhibitors. Toward this end, racemic mixtures of ten Mev analogues (1-10, Table 1) were synthesized chemically (9), each with a different substituent replacing the C_3 -methyl of mevalonate. Analogues 1, 3, 6, 7, and 9 (*i.e.* those with small planar substituents) were enzymat-

S. pneumoniae Mevalonate Pathway Enzymes

ically phosphorylated to the mono- (**X•p**) and diphosphorylated (**X•pp**) forms and purified by anion-exchange chromatography (see “Experimental Procedures”). Because MK and PMK only act on the (*R*)-isomer (**20**), the mono- and diphosphorylated products are stereochemically pure. Pure (*R*)-Mev analogues were obtained by treating the (*R*)-Mev•pp analogues (synthesized enzymatically) with alkaline phosphatase and purifying as above. The monophosphorylated forms of five of the analogues (**2**, **4**, **5**, **8**, and **10**, indicated by a dot (●) in Table 1) could not be produced enzymatically (**9**), and were not pursued further. However, racemic mixtures of the diphosphorylated forms of these analogues were synthesized chemically starting from the corresponding lactones and used to probe the structural constraints of the allosteric pocket of MK and the active site of DPM-DC (for a full description see [supplemental material](#)). Thus, of the 30 possible analogues (*i.e.* the non-, mono-, and diphosphorylated forms of each of the 10 analogue backbones), 25 were synthesized, purified, and tested as substrates and allosteric inhibitors of the Mev pathway enzymes.

Mevalonate Analogues as Substrates of GHMP Kinases—The ability of the Mev pathway GHMP kinases to accept alternative substrates was probed using the 25 Mev analogues listed in Table 1. Kinetic parameters for each enzyme-substrate pair were determined by analysis of complete reaction progress curves. Reactions were monitored using absorbance or fluorescence by stoichiometrically coupling (1:1) the production of ADP to the reduction of NADH, employing the well established pyruvate kinase/lactate dehydrogenase (PK/LDH) coupled assay system (**12**). The activity of PK regenerates the nucleotide, so the steady-state concentration of ATP is essentially fixed throughout the reaction. For MK and PMK, phosphorylated products were removed by the addition of downstream Mev pathway enzymes, obviating possible product inhibition. For DPM-DC, progress curves generated in the presence and absence of decarboxylated products had identical curvatures, indicating an absence of product inhibition under assay conditions (data not shown). Therefore, product *versus* time curves were fit directly to the integrated Michaelis-Menten equation (Equation 1 (**21**)) to extract k_{cat} and K_m (Table 1).

Substrate selectivity varied widely across the three GHMP kinases. MK and PMK showed similar trends in catalytic efficiency, accepting small, planar substituents (**6**) and excluding larger, branched substituents (**2**, **4**, **5**, **8**, and **10**). However, PMK generally exhibited lower K_m and higher k_{cat}/K_m values than MK for its substrates (see Table 1), indicating a relaxation of substrate selectivity in the second step of the pathway. DPM-DC was the least discriminating of the three enzymes, accepting all ten analogs as substrates. DPM-DC kinetic parameters for **1•pp**, **6•pp**, and **7•pp** were similar to those for Mev•pp, indicating excellent tolerance of a variety of small substituents. For larger substituents, branching played an important role in determining substrate selectivity, with unbranched compounds favored over branched ones. Branched analogs (**2•pp**, **4•pp**, and **10•pp**) showed greater than 14-fold decreased affinity compared with the native substrate, whereas unbranched and cyclic analogues (**3•pp** and **9•pp**, respectively) had K_m values similar to that of Mev•pp. The binding pocket is apparently limited to three-carbon substituents, shown by the strongly

reduced k_{cat}/K_m values for **4•pp** and **5•pp**. The substrate selectivity trend in DPM-DC is fundamentally different from that of MK and PMK, suggesting that substrate recognition is altered in this family member. This is perhaps not surprising, given that the Mev moiety is being phosphorylated on a different hydroxyl group in DPM-DC, requiring that the geometry of the binding pocket relative to ATP be substantially different from the other enzymes.

Structural Determinants of Substrate Selectivity—To ascertain whether active-site structural factors might explain the substrate selectivity of the Mev pathway enzymes, the active sites of all three enzymes were compared in the vicinity of the C_3 -methyl group of Mev, Mev•p, and Mev•pp. In the case of MK and PMK, co-crystal structures of the *S. pneumoniae* enzymes with bound acceptor ligands were available (PDB: 2OI2 and 3GON) (**8**, **22**). There are no ligand-bound structures of DPM-DC; however, Byres *et al.* have positioned Mev•pp in the *T. brucei* DPM-DC. Byres *et al.* used a number of criteria (**18**), including positioning the C_3 -hydroxyl to attack the γ -phosphate of ATP via interactions with conserved residues known to activate chemistry in GHMP kinases, the presence of an ordered sulfate interacting with conserved active-site residues (this sulfate was presumed to occupy the binding pocket for the terminal phosphate of Mev•pp) and an Arg that is well positioned in all DPM-DC structures to interact with the C_1 -carboxylate of Mev•pp. In addition, we note that, in the three GHMP kinase structures that contain bound Mev, Mev•p, or Mev•pp, the C_1 -carboxylate interacts with a conserved serine. This same Ser is present in each of the seven DPM-DC structures, and positioning Mev•pp according to the Byres *et al.* rationale places the carboxylate within contact distance of that Ser. These conserved anchor points were used to position Mev•pp in our *S. pneumoniae* model (see Fig. 3C), which was generated from the crystal structure of *S. pyogenes* DPM-DC (PDB: 2GS8) using Swiss PDB Viewer (**17**). The sequence of the *S. pyogenes* DPM-DC is 70% identical to that of the *S. pneumoniae* enzyme.

A comparison of these models highlights differences in the active site near the C_3 -methyl group across these enzymes (Fig. 3). The narrow selectivity seen in MK seems likely due to the fact that the C_3 -methyl points into a shallow depression anchored by the side chain of His-20, a highly conserved MK residue (Fig. 3A) that appears to be fixed in its orientation by a hydrogen-bonded network that includes the main-chain carbonyls of Gly-256 and His-20, the amide of Val-23, and a crystallographic water (Fig. 3A). This configuration places the C_3 -methyl in van der Waals contact with residues lining the C_3 -binding pocket and leaves little room to admit larger R-groups.

Similar to the interactions seen in the MK•Mev structure, the C_3 -methyl group of Mev•p resides in a shallow, “tight” binding pocket in PMK. In this case, the C_3 -methyl is directed toward a tyrosine side chain (Tyr-16) that occupies a position analogous to that of His-20 in MK (Fig. 3B). However, instead of a hydrogen-bonded network, Tyr-16 is embedded in a hydrophobic pocket composed of Glu-15, Met-216, Val-217, Ile-220, Ile-224, Leu-265, Ile-269, and Ala-293. Although these structures offer little definitive evidence to explain the somewhat relaxed selectivity of PMK over MK, it is interesting to consider that a hydro-

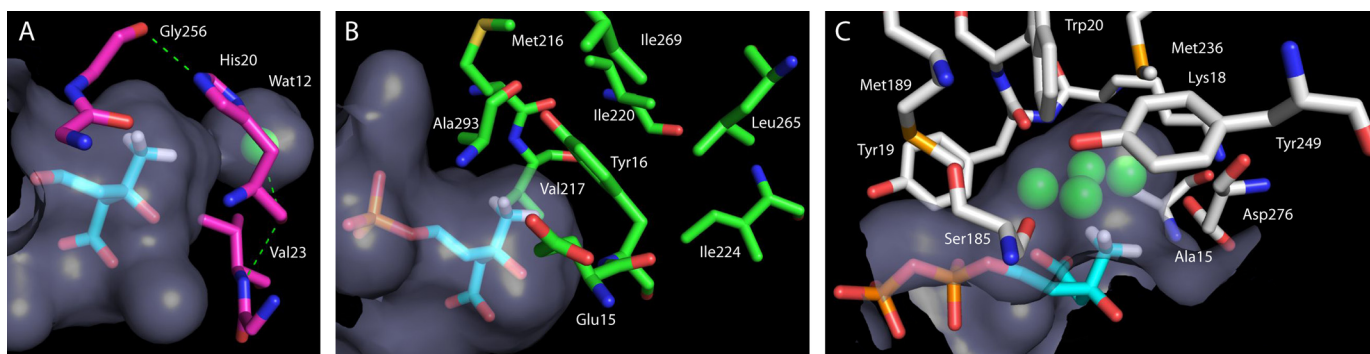


FIGURE 3. Structural determinants of substrate selectivity in the mevalonate pathway. Models of the Mev pathway enzymes are shown with their respective acceptor substrates bound to the active site. Surfaces (light blue) represent the van der Waals contact surface of the protein model. Substrates Mev, Mev-p, and Mev-pp are shown in stick representation and colored by atom type: C in cyan, H in white, O in red, and P in orange. The C₃-methyl group is shown with hydrogens attached. *A*, *S. pneumoniae* MK (magenta, PDB: 2O12) bound to Mev. The Mev C₃-methyl group points toward His-20, which forms a hydrogen-bonded network (green dashes) with a water molecule (green sphere), Gly-256, and Val-23. *B*, *S. pneumoniae* PMK (green, PDB: 3GON) with Mev-p. The Mev-p C₃-methyl group points toward a hydrophobic network capped by Tyr-19. *C*, homology model of *S. pneumoniae* DPM-DC based on the *S. pyogenes* DPM-DC (white, PDB: 2G58) with Mev-pp manually positioned (see “Experimental Procedures”). The Mev-pp C₃-methyl points into a large water-filled cavity composed of nine conserved residues. Images were generated by using PyMOL (19).

phobic pocket may have greater flexibility than one linked by hydrogen bonds (23, 24).

In contrast to MK and PMK, our model of the DPM-DC·Mev·pp complex directs the C₃-methyl group into a deep, narrow hydrophilic cavity that contains four crystallographic water molecules in the apo structure (Fig. 3C). Inspection of the seven DPM-DC homologues in the PDB revealed that the structure of the C₃-cavity and the residues that define it are remarkably well conserved across prokaryotes and eukaryotes. The volume of the cavity is capable of accommodating two-carbon *R*-groups without steric strain, three-carbon *R*-groups will likely result in a “snug” fit, whereas larger substituents are unlikely to access the pocket well. This simple analysis of the C₃-pocket accessibility predicts the behavior of the enzyme toward the C₃ analogues well (see Table 1) and supports the validity of the model. It is interesting to consider that this expanded cavity, which extends the substrate repertoire of the enzyme at C₃, may provide the cell with the means to decarboxylate other, as yet unidentified, β-hydroxy carboxylic acids.

Mev·pp Analogues as Allosteric Inhibitors of MK—The ten diphosphorylated analogues (Table 1) were designed to probe the structure of the allosteric site of MK. A preliminary study was carried out in which all ten compounds were screened at 250 μM for MK inhibition at fixed concentrations of substrates. Compounds that inhibited MK activity by <1% at this level (2·pp, 4·pp, 5·pp, and 10·pp) were not considered further. For compounds exhibiting detectable inhibition at 250 μM, a titration was carried out to determine the IC₅₀ (Table 2 and “Experimental Procedures”). MK inhibitors fell into three broad groups based on their IC₅₀ values relative to that of Mev·pp: ~50-fold higher (6·pp and 9·pp), ~250-fold higher (1·pp, 7·pp, and 8·pp), and ~900-fold higher (3·pp). Although we expect that this inhibition represents binding of a ligand at the allosteric site, it is formally possible that the analogue (X·pp), which resembles the acceptor (X) bound to the β- and γ-phosphates of ATP, could act as a bisubstrate inhibitor, in which case it is predicted to compete with the substrates. To distinguish between these possibilities, the inhibition mechanism of the two best inhibitors, 6·pp and 9·pp, was determined in a classic

TABLE 2
Steady-state inhibition of *S. pneumoniae* MK

Inhibitor	IC ₅₀
	μM
Mev·pp	0.98 (0.01)
1·pp	250 (1)
2·pp	— ^a
3·pp	900 (1)
4·pp	— ^a
5·pp	— ^a
6·pp	50 (1)
7·pp	200 (1)
8·pp	240 (1)
9·pp	44 (1)
10·pp	— ^a

^a Compound inhibited enzyme turnover by <1% at a concentration of 250 μM. Parenthetical values indicate standard error.

TABLE 3
Initial rate parameters for *S. pneumoniae* MK in the presence of X·pp

Inhibitor	K _{m-Mev}	K _{is-Mev} ^a	K _{ii-Mev}	K _{m-ATP}	K _{is-ATP}	K _{ii-ATP}
	μM	μM	μM	μM	μM	μM
6·pp	25 (1) ^b	76 (2)	75 (3)	0.98 (0.05)	43 (6)	45 (3)
9·pp	23 (3)	58 (3)	55 (5)	0.98 (0.05)	59 (6)	65 (5)

^a K_{is} and K_{ii} are the steady-state affinities of the inhibitor for the E·S2 and E·S1·S2 complexes, respectively, where S1 and S2 are the non-variable and variable substrates, respectively (see “Experimental Procedures”).

^b Standard errors are enclosed in parentheses.

initial rate study in which the concentration of one substrate (Mev or ATP, four values spanning the K_m values) was varied against the concentration of inhibitor (three values spanning the K_i) (see supplemental Fig. S1). A noncompetitive reversible inhibition model provided the best fit to each data set (Table 3). Pure noncompetitive inhibition by 6·pp and 9·pp against both substrates, as indicated by identical K_{is} and K_{ii} values (within error), is diagnostic of an allosteric inhibition mechanism (13, 25). These results indicate that X·pp inhibition is due to binding at the allosteric site.

The X·pp analogues are relatively weak inhibitors, suggesting that the allosteric binding pocket does not tolerate substitution of the Mev·pp C₃-methyl group by larger moieties. The shape of the pocket is difficult to infer, because the IC₅₀ values do not correlate with the size or flexibility of the C₃ substituents. For example, among analogues with two-carbon substituents, the

S. pneumoniae Mevalonate Pathway Enzymes

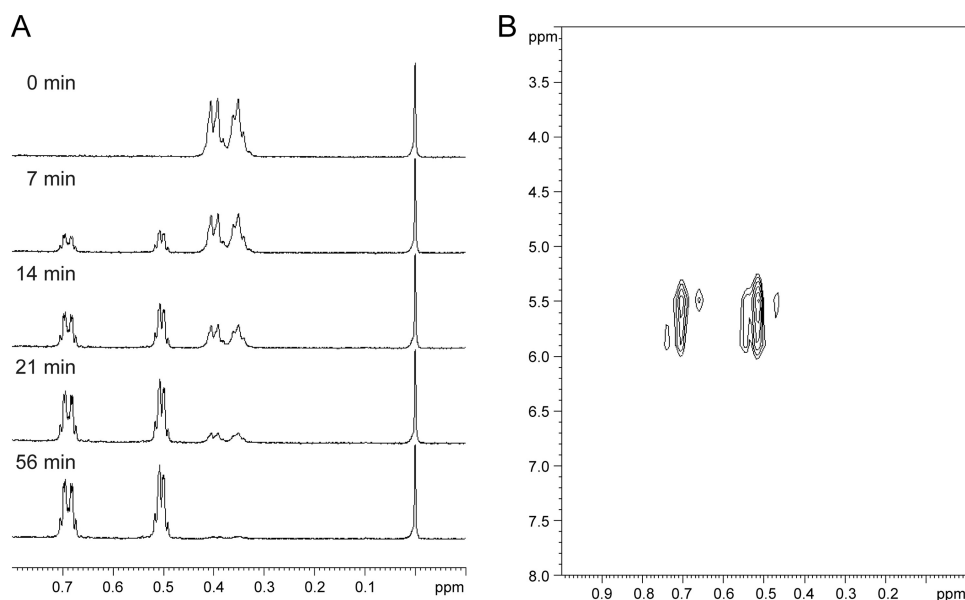


FIGURE 4. NMR determination of the fate of the cyclopropyl ring. A, partial one-dimensional ¹H NMR spectra at 600 MHz obtained at various times during the enzymatic reaction of **9**·pp with DPM-DC. A spectrum was taken every 7 min after the addition of enzyme. The time stamp of a given reaction time is shown. The multiplets at 0.40 ppm/0.35 ppm and at 0.69 ppm/0.50 ppm represent the cyclopropyl methylene protons of the starting material and product, respectively. The integrated areas of the multiplets are preserved during the reaction indicating that all starting material is converted to product. B, expansion of two-dimensional ¹H-¹³C HSQC with multiplicity editing of the product after enzymatic reaction of **9**·pp. The signals at 0.69 ppm (¹H)/5.5 ppm (¹³C) and at 0.50 ppm (¹H)/5.5 ppm (¹³C) are from the methylene protons of the cyclopropyl ring. These chemical shifts are characteristic of a cyclopropyl ring and demonstrate that the ring is preserved during the enzymatic reaction.

vinyl analogue (**6**·pp) inhibits MK 4- to 5-fold better than either the ethyl (**1**·pp) or ethynyl (**7**·pp) analogues, suggesting that some subtle combination of size, geometry, and electrophilicity makes the vinyl group preferred. Analogues with three-carbon substituents appear to inhibit differently on the basis of shape: linear **8**·pp outperforms the more flexible **3**·pp. Surprisingly, the vinyl and cyclopropyl (**9**·pp) analogues inhibit equally well, despite the addition of a carbon in **9**·pp and the exclusion of all other branched substituents. This result suggests that the region of the allosteric site that binds the C₃ substituent is highly sensitive to the geometry of the group and that favorable electronic interactions between the enzyme and the π-orbitals in the vinyl group and the cyclopropyl ring may contribute to binding affinity.

This study revealed that our prodrug strategy for MK inhibition will be limited to Mev analogues with small C₃ substituents. Fluorinated Mev·pp analogues, which are isosteric with Mev·pp, are inhibitors of mammalian DPM-DC and should be excellent inhibitors of *S. pneumoniae* MK (26, 27).

Mev·pp Analogues as Probes of DPM-DC Reaction Mechanism—Five analogues (**6**·pp through **10**·pp) were designed to covalently inactivate DPM-DC by forming a highly reactive carbocation capable of covalent attachment at the active site (see the introduction and Fig. 2). These compounds did not detectably inactivate the enzyme under the initial rate conditions used to measure their kinetic constants as substrates of DPM-DC (see “Mevalonate Analogues as Substrates of GHMP Kinases”). To assess whether inactivation was too slow to detect in the initial rate experiments, the DPM-DC reaction conditions were adjusted (see “Experimental Procedures”) so that the concentration of the analogue would remain saturating during

>1000 turnovers of the enzyme. With each analogue, the rates of reaction before and after 1000 turnovers were identical, within experimental error, indicating that ≤4% of the enzyme was inactivated during the measurement. Thus, either the analogues are decarboxylated (like Mev·pp) or the carbocation reacts with water to form non-decarboxylated products.

To determine the fate of the analogues, we focused on the cyclopropyl derivative (**9**·pp), which we expected to inactivate DPM-DC via opening of the strained three-membered ring (28). When a tertiary carbocation forms adjacent to a cyclopropyl ring, it is expected to rearrange into a homoallyl cation (see Fig. 2) that is stabilized due to release of 27 kcal/mol ring strain (29, 30). If the homoallyl cation were to react with water (rather than the protein) at the active site, the reaction would produce a ring-opened primary alcohol that can be readily

identified by NMR spectrometry due to the large chemical shift differences between cyclopropyl protons and their linear counterparts (31). An NMR experiment that monitored the cyclopropyl proton resonances during product formation revealed that the substrate peaks are shifted only slightly downfield (~0.3 ppm) in the product. The sum of the integrated intensities of the substrate and product resonances remained fixed throughout the experiment (Fig. 4). An HSQC experiment identified the product resonances (0.5 and 0.68 ppm, Fig. 4A) as those of cyclopropyl ring protons (Fig. 4B). Furthermore, the cyclopropyl protons in the product showed long range correlations to carbons at 107.6 ppm and 148.3 ppm (two-dimensional ¹H-¹³C HMBC (32); data not shown), indicating that a double bond is adjacent to the cyclopropyl ring, which confirmed that the product results from decarboxylation. These NMR data rule out a ring-opened product and support the analogue undergoing a decarboxylation that resembles that of the native substrate, Mev·pp.

These results call into question the extent of carbocation formation in the DPM-DC transition state. If a full carbocation had formed, we expected to observe rearrangement of the cyclopropyl group. If no nucleophile is in close proximity to the carbocation (the protein surface or water), we might expect to see only intact cyclopropyl products; however, the presence of four crystallographic water molecules in the large pocket adjacent to C₃ and the proximity of the Asp-276, Lys-18, Ser-185, and Met-189 side chains and the Tyr-19 carbonyl as potential nucleophiles argue against this possibility (Fig. 3C). Alternatively, carbocation formation may be minimal or absent, in which case elimination of the carboxylate and the phosphate is concerted rather than dissociative. Abeles' work on the effects

of altered electron induction at C_3 with the mammalian enzyme shows clearly that DPM-DC chemistry is sensitive to such changes and supports the development of a positive charge at C_3 in the transition state (10). Further, by replacing C_3 with a positively charged amine, he created an analogue that mimicked the structure and charge characteristics of a dissociative transition state. The affinity of this analogue ($0.75 \mu\text{M}$) was only 20-fold higher than that of the substrate (33), which, while supportive of a dissociative character in the transition state, is perhaps more consistent with development of partial rather than complete positive charge at C_3 . Although studies that correlate the extent of positive charge formation with degree of ring opening in cyclopropyl ring systems do not yet exist, our results, which demonstrate no detectible ring opening, are consistent with only slight positive charge formation in the transition state. Using kinetic isotope effects, it may be possible to assess the extent of positive charge development on C_3 at the transition state.

Targeting the Human DPM-DC—Exclusive of their effects on bacterial enzymes, the Mev^{pp} analogues might also inhibit the human DPM-DC, because it is not clear whether the corresponding human and bacterial enzymes have diverged to the point where they could be targeted orthogonally, as is the case for MK. Inhibitors of the human Mev pathway (statins and bisphosphonates) are used clinically to reduce cholesterol biosynthesis, increase bone density, and decrease cell proliferation in cancer (34). Down-regulation of the human Mev pathway by statins has recently been linked to disruption of replication by hepatitis C virus (35, 36) and human immunodeficiency virus (37), enhancement of anticancer drugs (38), and anti-inflammatory effects in the lung and airways (39, 40). These findings suggest that DPM-DC inhibitors may find additional uses in the treatment of non-infectious diseases, which obviates the need for selective DPM-DC inhibition.

Conclusions—Twenty-five novel Mev analogues have been tested as substrates and inhibitors of three enzymes that comprise the Mev pathway in *S. pneumoniae*. Although the MK allosteric binding pocket admits certain analogues, it is highly selective for Mev^{pp}. Substrate selectivity of the enzymes varies considerably across the pathway, with MK providing the most stringent selection. The active-site structures of the Mev pathway GHMP kinases provide a rationale for the substrate selectivity of these enzymes toward substitution at C_3 . The C_3 R-group pocket in DPM-DC is considerably larger than that of MK or PMK, and the volume of this cavity correlates well with selectivity toward R-group substitution. The high conservation of this pocket indicates that it has been evolutionarily maintained, and that the ability to decarboxylate substrates that vary at the C_3 R-group may provide an important metabolic function. Finally, results using analogues designed to act as mechanism-based inhibitors of DPM-DC suggest that ionization of phosphate and decarboxylation of the p-Mev^{pp} intermediate occurs in a concerted fashion with little carbocation development at C_3 .

REFERENCES

- Obaro, S., and Adegbola, R. (2002) *J. Med. Microbiol.* **51**, 98–104
- Schuchat, A., Robinson, K., Wenger, J. D., Harrison, L. H., Farley, M., Reingold, A. L., Lefkowitz, L., and Perkins, B. A. (1997) *N. Engl. J. Med.* **337**, 970–976
- Van Bambeke, F., Reinert, R. R., Appelbaum, P. C., Tulkens, P. M., and Peetermans, W. E. (2007) *Drugs* **67**, 2355–2382
- Kyaw, M. H., Lynfield, R., Schaffner, W., Craig, A. S., Hadler, J., Reingold, A., Thomas, A. R., Harrison, L. H., Bennett, N. M., Farley, M. M., Facklam, R. R., Jorgensen, J. H., Besser, J., Zell, E. R., Schuchat, A., and Whitney, C. G. (2006) *N. Engl. J. Med.* **354**, 1455–1463
- Huang, S. S., Hinrichsen, V. L., Stevenson, A. E., Rifas-Shiman, S. L., Kleinman, K., Pelton, S. I., Lipsitch, M., Hanage, W. P., Lee, G. M., and Finkelstein, J. A. (2009) *Pediatrics* **124**, e1–e11
- Wilding, E. I., Brown, J. R., Bryant, A. P., Chalker, A. F., Holmes, D. J., Ingraham, K. A., Iordanescu, S., So, C. Y., Rosenberg, M., and Gwynn, M. N. (2000) *J. Bacteriol.* **182**, 4319–4327
- Lange, B. M., Rujan, T., Martin, W., and Croteau, R. (2000) *Proc. Natl. Acad. Sci. U.S.A.* **97**, 13172–13177
- Andreassi, J. L., 2nd, Bilder, P. W., Vetting, M. W., Roderick, S. L., and Leyh, T. S. (2007) *Protein Sci.* **16**, 983–989
- Kudoh, T., Park, C. S., Lefurgy, S. T., Sun, M., Michels, T., Leyh, T. S., and Silverman, R. B. (2010) *Bioorg. Med. Chem.* **18**, 1124–1134
- Dhe-Paganon, S., Magrath, J., and Abeles, R. H. (1994) *Biochemistry* **33**, 13355–13362
- Pilloff, D., Dabovic, K., Romanowski, M. J., Bonanno, J. B., Doherty, M., Burley, S. K., and Leyh, T. S. (2003) *J. Biol. Chem.* **278**, 4510–4515
- Tchen, T. T. (1958) *J. Biol. Chem.* **233**, 1100–1103
- Andreassi, J. L., 2nd, Dabovic, K., and Leyh, T. S. (2004) *Biochemistry* **43**, 16461–16466
- McClure, W. R. (1969) *Biochemistry* **8**, 2782–2786
- Cleland, W. W. (1967) *Adv. Enzymol. Relat. Areas Mol. Biol.* **29**, 1–32
- Mandel, J. (1964) *The Statistical Analysis of Experimental Data*, pp. 131–159, Dover, New York
- Guex, N., and Peitsch, M. C. (1997) *Electrophoresis* **18**, 2714–2723
- Byres, E., Alphey, M. S., Smith, T. K., and Hunter, W. N. (2007) *J. Mol. Biol.* **371**, 540–553
- DeLano, W. L. (2002) *The PyMOL Molecular Graphics System*, DeLano Scientific LLC, San Carlos, CA
- Cornforth, R. H., Fletcher, K., Hellig, H., and Popjak, G. (1960) *Nature* **185**, 923–924
- London, J. W., Shaw, L. M., and Garfinkel, D. (1977) *Anal. Chem.* **49**, 1716–1719
- Andreassi, J. L., 2nd, Vetting, M. W., Bilder, P. W., Roderick, S. L., and Leyh, T. S. (2009) *Biochemistry* **48**, 6461–6468
- Davis, A. M., and Teague, S. J. (1999) *Angew. Chem. Int. Ed. Engl.* **122**, 736–749
- Kawaguchi, S., Nobe, Y., Yasuoka, J., Wakamiya, T., Kusumoto, S., and Kuramitsu, S. (1997) *J. Biochem.* **122**, 55–63
- Cleland, W. W. (1963) *Biochim. Biophys. Acta* **67**, 173–187
- Qiu, Y., and Li, D. (2006) *Biochim. Biophys. Acta* **1760**, 1080–1087
- Reardon, J. E., and Abeles, R. H. (1987) *Biochemistry* **26**, 4717–4722
- Suckling, C. J. (1988) *Angew. Chem. Int. Ed. Engl.* **27**, 537–552
- Hart, H., and Sandri, J. M. (1959) *J. Am. Chem. Soc.* **81**, 320–326
- Liebman, J. F., and Greenberg, A. (1976) *Chem. Rev.* **76**, 311–365
- Gunther, H. (1997) *NMR Spectroscopy: Basic Principles, Concepts, and Applications in Chemistry*, John Wiley & Sons, New York
- Bax, A., and Summers, M. F. (1986) *J. Am. Chem. Soc.* **108**, 2093–2094
- Wolfenden, R. (1999) *Bioorg. Med. Chem.* **7**, 647–652
- Buhaescu, I., and Izzedine, H. (2007) *Clin. Biochem.* **40**, 575–584
- Lyn, R. K., Kennedy, D. C., Sagan, S. M., Blais, D. R., Rouleau, Y., Pegoraro, A. F., Xie, X. S., Stolow, A., and Pezacki, J. P. (2009) *Virology* **394**, 130–142
- Ye, J., Wang, C., Sumpter, R., Jr., Brown, M. S., Goldstein, J. L., and Gale, M., Jr. (2003) *Proc. Natl. Acad. Sci. U.S.A.* **100**, 15865–15870
- del Real, G., Jiménez-Baranda, S., Mira, E., Lacalle, R. A., Lucas, P., Gümez-Moutün, C., Alegret, M., Peña, J. M., Rodríguez-Zapata, M., Alvarez-Mon, M., Martínez, A. C., and Mañes, S. (2004) *J. Exp. Med.* **200**, 541–547
- Fritz, G. (2009) *Curr. Cancer Drug Targets* **9**, 626–638
- Camoretti-Mercado, B. (2009) *Transl. Res.* **154**, 165–174
- Zeki, A. A., Franzi, L., Last, J., and Kenyon, N. J. (2009) *Am J. Respir. Crit. Care Med.* **180**, 731–740